PERFORMANCE INVESTIGATION AND OPTIMIZATION OF A MICROCHANNEL HEAT EXCHANGER WITH HYBRID FINS

Xin GU, Junjie Li, Jinting ZHANG, Weijie CHEN, Yongqing WANG*

School of Mechanical and Power Engineering, Zhengzhou University, Zhengzhou 450001, China

* Corresponding author, E-mail address: wangyq@zzu.edu.cn

Printed circuit board heat exchangers have demonstrated great potential for application in supercritical carbon dioxide Brayton cycles due to their highly efficient and compact structural characteristics. However, conventional single-fin designs often suffer from flow separation and stagnation under complex conditions, limiting thermal performance. This study introduces a novel hybrid fin design that integrates smooth airfoil and diamond-shaped fins. Using a unit microchannel model, the thermal-hydraulic performance of smooth airfoil, diamond-shaped, and hybrid fin channels was numerically evaluated. Results show that the hybrid configuration achieves synergistic balance between enhanced heat transfer and reduced flow resistance. Within an inlet mass flow rate of 0.00121–0.00323 kg/s, corresponding to Reynolds number of 3200–7200, the hybrid channel increases the Nusselt number by 16.5–10.4% and 9.2–4.6% compared to the smooth airfoil and diamond-shaped channels, respectively. Moreover, it exhibits improvements in the Nusselt number to the friction factor ratio of 5.7–10.7% over the smooth airfoil channel and 9.8–16.4% over the diamond-shaped channel. The overall thermo-hydraulic efficiency $Q/\Delta p$, the ratio of the heat transfer rate to pressure drop, is also enhanced by 2.3–9.7% and 6.3–33.5%, respectively. Thus, the hybrid design effectively optimizes the trade-off between heat transfer and pressure drop, offering valuable insights for the structural design and parameter optimization of printed circuit heat exchangers.

Keywords: *Hybrid-fin microchannel; PCHE; thermo-hydraulic performance; structural optimization*

1. Introduction

With the accelerating pace of global industrialization and the continuous growth of energy demand, developing high-efficiency and energy-saving heat exchange equipment has become a key task in industrial production and energy conversion systems. Microchannel heat exchangers are commonly manufactured using Printed Circuit Heat Exchanger (PCHE) technology. In the supercritical carbon dioxide (sCO_2) Brayton cycle, PCHE play an essential role by significantly improving heat exchange efficiency and energy utilization [1]. Compared with traditional systems such as air Brayton and steam Rankine cycles, the sCO_2 Brayton cycle achieves higher cycle efficiency with the aid of PCHE. As the sCO_2 Brayton cycle becomes increasingly widespread in advanced energy systems, the demand for high-performance heat exchangers continues to rise, posing new challenges for further improving overall cycle efficiency [2, 3]. PCHE not only enhance thermal efficiency and energy utilization, but also feature

compactness, small volume, and light weight [4]. However, to fully exploit these advantages under diverse operating conditions, optimizing the microchannel geometry of PCHE remains an important research focus [5].

sCO₂ with its high density, low viscosity, and high thermal conductivity, is a promising PCHE working fluid, especially in continuous channel studies, and has attracted growing attention in advanced energy systems [6, 7]. Chu et al. [8] compared the heat transfer and pressure drop characteristics of *sCO₂* and water in straight-channel PCHE, showing that *sCO₂* exhibits superior heat transfer performance but experiences up to 17.6% performance degradation under trans-critical conditions due to drastic property variations. Figley et al. [9]. analyzed the thermo-hydraulic characteristics of a semicircular-channel PCHE under various mass flow rates, revealing that the critical Reynolds number exceeds the conventional threshold of 2300. Meshram et al. [10] systematically compared straight and zigzag PCHE under fully turbulent conditions and found that the zigzag configuration reduces exchanger volume significantly but at the cost of higher-pressure losses. Regarding channel cross-sectional geometry, Lee and Kimi [11] compared semicircular, rectangular, trapezoidal, and circular sections and concluded that rectangular sections yield the best heat transfer performance but the poorest hydraulic performance, while circular channels demonstrate the opposite trend. Ngo et al. [12] developed a novel S-shaped fin PCHE for hot-water systems, achieving a 37% reduction in CO_2-side pressure drop and an order-of-magnitude decrease on the water side, while maintaining compactness.

Research on heat transfer enhancement has increasingly focused on non-continuous PCHE channels, especially the design and arrangement of fins, which strongly affect thermo-hydraulic performance [13, 14]. Zhang et al. [15] numerically investigated a novel airfoil-fin PCHE and found that its pressure drop was only one-sixth of that in a serrated channel, demonstrating the potential of discontinuous fins for drag reduction. Yang et al. [16] found that diamond-fin channels can achieve a comparable volumetric heat transfer rate to serrated channels at much lower pressure drops, highlighting the critical role of fin geometry. Kim et al. [17] examined different arrangements of airfoil fins, including staggered configurations and variations in horizontal and vertical spacing, and reported that the fully staggered arrangement provides the best comprehensive performance. Chang et al. [18] investigated asymmetric airfoil-fin PCHE using *sCO₂*, finding that average thermal resistance is a more sensitive metric than total resistance for evaluating thermal performance. Cui et al. [19] showed that staggered fins can reduce boundary layer effects and improve heat transfer efficiency.

In terms of comprehensive fin geometry and positioning optimization, Wu et al. [20] proposed a hybrid configuration combining swordfish-shaped and diamond-shaped fins in an alternating pattern, demonstrating that adjusting the lateral spacing L_b and longitudinal spacing L_c can effectively enhance heat transfer under constrained pressure drops. Zhao et al. [21] numerically studied the influence of airfoil-fin arrangements on the thermo-hydraulic performance of supercritical nitrogen in PCHE, showing that reducing the staggered distance L_s and lateral spacing L_v can further enhance heat transfer. Xu et al. [22] reported that fin arrangement has little effect at low mass flow rates, but during heating, density reduction increases flow velocity and resistance, aggravating separation and stagnation losses, while viscosity plays a minor role. These studies suggest that hybrid fin arrangements represent an inevitable trend in performance optimization.

The advancement of *sCO₂* Brayton cycles necessitates high-performance heat exchangers. To mitigate the common problem of flow separation encountered in conventional single-fin designs, a novel hybrid-fin configuration is proposed that incorporates an alternating arrangement of smooth airfoil and

diamond-shaped fins. This structure aims to improve the overall thermo-hydraulic performance of printed circuit heat exchangers within sCO_2 Brayton cycles. Using sCO_2 as the working fluid, its thermo-hydraulic performance is systematically compared with single-fin channels across Reynolds number (*Re*) of 3200 to 7200. The hybrid design demonstrates superior synergy between heat transfer enhancement and pressure drop, by using the performance evaluation criteria, the ratio of Nusselt number (*Nu*) to friction factor (*f*) *Nu/f* and $Q/\Delta p$, to evaluate the balance between heat transfer enhancement and flow resistance, along with local flow analysis, thereby offering practical guidance for high-efficiency sCO_2 systems.

2. Methodology and numerical model

2.1. Development of the hybrid-fin microchannel heat exchanger structure

The conventional PCHE model with traditional airfoil fins is shown in Fig. 1, where the hot and c old fluid paths are indicated. The smooth airfoil fin [23] enhances local convection through small-scale vortices and flow-guiding effects, providing moderate disturbance with smooth flow and low pressure drop, making it suitable for high-speed or low-viscosity flows requiring efficient heat transfer. In contr ast, the diamond-shaped fin [24], disrupts the thermal boundary layer with its protruded structure, prom oting strong local mixing and guided flow to improve heat transfer uniformity, especially under low *Re* or high-viscosity conditions.

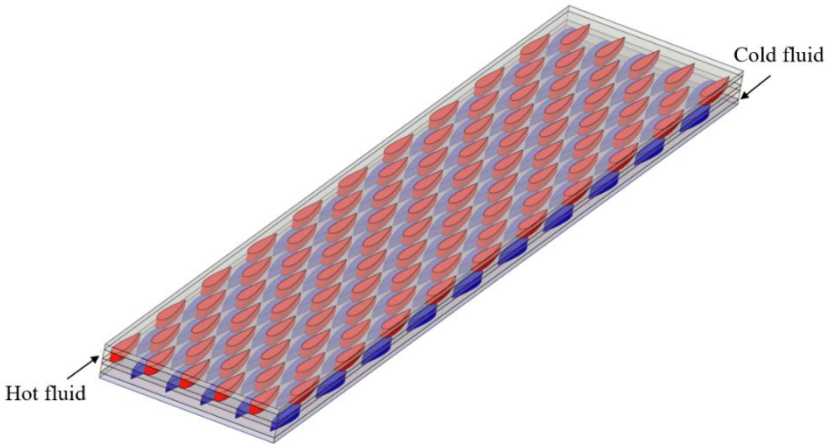

Fig. 1. Unit model for PCHE

2.2. Numerical model and geometric parameters

To combine the advantages of both fin types, this study proposes a hybrid-fin microchannel heat e xchanger, in which smooth airfoil fins and diamond-shaped fins are alternately arranged. The structural configuration is illustrated in Fig. 2. Fig. 2 (a) presents the hybrid-fin configuration, where smooth airf oil and diamond fins are staggered to form a mixed arrangement; Fig. 2 (b) shows the single smooth ai rfoil-fin channel; and Fig. 2 (c) depicts the single diamond-fin channel.

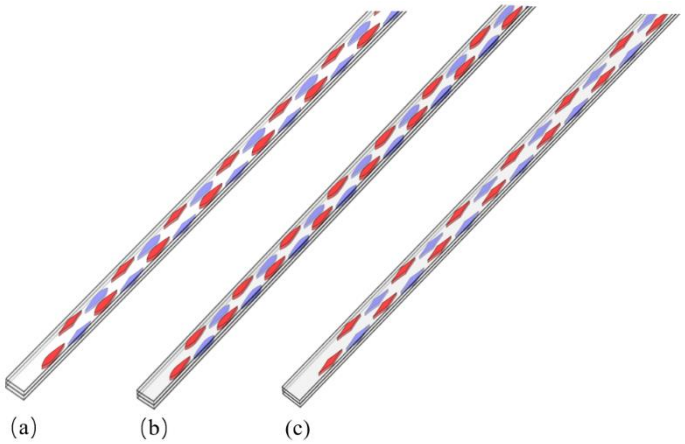

Fig. 2. Schematic diagram of a simplified model of PCHE (a) hybrid fin channel, (b) Smooth airfoil fin channel, and (c) Rhombus fin channel

The geometric configuration of the hybrid-fin channel is formed by the staggered arrangement of smooth airfoil fins and diamond-shaped fins. The top view of the studied model is shown in Fig. 3, and its characteristic dimensions are defined by the following parameters: L_a is total width of the channel; L_v is lateral spacing between adjacent fins of different types; L_h is lateral spacing between adjacent fins of the same type; L_s is longitudinal spacing between adjacent fins of different types. These parameters define the fin arrangement and are utilized to study the thermal-hydraulic performance of the channel. The geometrical parameters adopted in this study are set as follows: L_a is 4 mm, L_h is 14 mm, L_s is 2 m m, and L_v is 7 mm. Both fin types have a chord length of 6 mm and a maximum thickness of 1 mm.

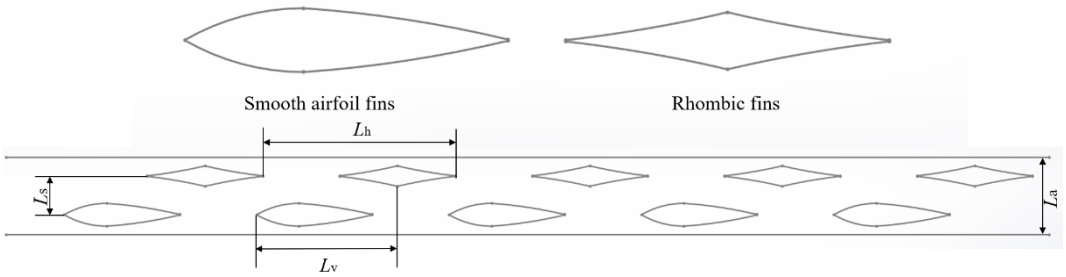

Fig. 3. Planar schematic diagram

2.3. Boundary conditions

The boundary conditions adopted in this study are summarized in Tab. 1. The cold-side fluid is water, with a mass flow inlet and an outlet pressure of 0.15 MPa. The inlet temperature of the cold fluid is 298.15 K. The hot-side fluid is sCO_2, also defined by a mass flow inlet. Five different inlet mass flow rates were selected: 0.00121 kg/s, 0.00188 kg/s, 0.00234 kg/s, 0.00279 kg/s, and 0.00323 kg/s, corresponding to *Re* ranging from 3200 to 7200. The inlet temperature of the hot fluid is 333 K, and the outlet pressure is set to 9.5 MPa. These boundary conditions are designed to simulate realistic operating states of PCHE within an sCO_2 Brayton cycle and to evaluate the thermal–hydraulic performance of the proposed hybrid-fin microchannel structure. Periodic boundary conditions represent the repetitive channel arrangement, while adiabatic external walls eliminate external heat transfer. Conjugate heat transfer is enforced at all fluid-solid interfaces.

Tab. 1. Boundary conditions

Hot side	Value	Cold side	Value
$T_{h,\,in}$ [K]	333	$T_{c,\,in}$ [K]	298.15
$p_{h,\,out}$ [MPa]	9.5	$p_{c,\,out}$ [MPa]	0.15
$m_{h,\,in,1}$ [kgs^{-1}]	0.00121		
$m_{h,\,in,2}$ [kgs^{-1}]	0.00188		
$m_{h,\,in,3}$ [kgs^{-1}]	0.00234	$m_{c,\,in}$ [kgs^{-1}]	0.00225
$m_{h,\,in,4}$ [kgs^{-1}]	0.00279		
$m_{h,\,in,5}$ [kgs^{-1}]	0.00323		

2.4. Numerical simulation setup

The numerical simulations employ appropriate boundary and physical settings to analyze flow and heat transfer in PCHE channels. Periodic boundary conditions are applied to the longitudinal and lateral walls to represent the repetitive channel structure, while adiabatic conditions on the front and rear walls eliminate external heat exchange. A conjugate heat transfer condition is enforced at fluid–solid interfaces. The thermophysical properties of *sCO₂* are obtained from the NIST REFPROP database, and the solid wall is 316L stainless steel. Simulations are performed using ANSYS Fluent with the SST k-ω turbulence model, which reliably captures near-wall flow characteristics, separation, and adverse pressure gradients in the transitional-to-turbulent regime between *Re* of 3200 and 7200. Pressure-velocity coupling is handled via the SIMPLE algorithm, and a second-order upwind scheme ensures numerical accuracy.

2.5. Governing equations

The governing equations used in this study are as follows:
Continuity equation:

$$\frac{\partial(\rho u)}{\partial x}+\frac{\partial(\rho v)}{\partial y}+\frac{\partial(\rho w)}{\partial z}=0 \tag{1}$$

where, u, v and w [ms^{-1}] are velocity vector of x, y and z direction.
Momentum equation:

$$\rho\frac{\partial(u_i u_j)}{\partial x_j}=-\frac{\partial p_i}{\partial x_j}+\mu\frac{\partial}{\partial x_j}+\mu\frac{\partial}{\partial x_j}\left(\frac{\partial u_i}{\partial x_j}+\frac{\partial u_j}{\partial u_i}-\frac{2}{3}\delta_{ij}\frac{\partial u_k}{\partial x_k}\right) \tag{2}$$

where p [Pa] is the pressure and, μ [Pa·s] is the dynamic viscosity of the fluid.
Energy equation:

$$u\frac{\partial t}{\partial x}+v\frac{\partial t}{2y}+w\frac{\partial t}{\partial z}=\frac{\lambda}{\rho c_P}\left(\frac{\partial^2 t}{\partial x^2}+\frac{\partial^2 t}{\partial y^2}+\frac{\partial^2 t}{\partial z^2}\right) \tag{3}$$

Where ρ [kgm^{-3}] is the fluid density, c_p [Jkg^{-1}K^{-1}] is the specific heat capacity, and λ [Wm^{-1}K^{-1}] is the thermal conductivity of the fluid.

Solid heat conduction equation:

$$\frac{\partial}{\partial x}\left(\lambda_s \frac{\partial T}{\partial x}\right)+\frac{\partial}{\partial y}\left(\lambda_s \frac{\partial T}{\partial y}\right)+\frac{\partial}{\partial z}\left(\lambda_s \frac{\partial T}{\partial z}\right)=0 \tag{4}$$

where λ_s [$Wm^{-1}K^{-1}$] is the thermal conductivity of the solid material, and T [K] is the temperature of the solid element.

The SST k-ω turbulence model is selected, described as follows:

k-equation:

$$\frac{\partial}{\partial x_i}(\rho k u_i)=\frac{\partial}{\partial x_i}\left(\left(\mu+\frac{\mu_t}{\sigma_k}\right)\frac{\partial k}{\partial x_j}\right)+G_k-Y_k \tag{5}$$

Ω-equation:

$$\frac{\partial}{\partial x_i}(\rho \omega u_i)=\frac{\partial}{\partial x_i}\left(\left(\mu+\frac{\mu_t}{\sigma_\omega}\right)\frac{\partial \omega}{\partial x_j}\right)+G_\omega-T_\omega+D_\omega \tag{6}$$

Where, G_k is the production of k, G_ω is the generation of ω, Y_k and T_ω are the dissipation terms of turbulent kinetic energy; D_ω represents the cross-diffusion term; σ_k and σ_ω are the dimensionless turbulent Prandtl numbers, with values of σ_k=1.0, σ_ω=1.3.

3. Mesh independence analysis and model validation

3.1. Mesh independence verification

A mesh independence study was performed for the hybrid channel PCHE model. For the configuration with L_h = 14 mm and L_s = 2 mm, five mesh densities were tested, ranging from 1.1 to 8.2 million cells. The mesh with 3.46 million cells is shown in Fig. 4. As seen in Fig. 5, both the temperature difference and pressure drop stabilize with mesh refinement. When the cell count exceeds two million, variations in these quantities remain below 1%, confirming satisfactory grid convergence. Thus, the mesh with 3.46 million cells was selected for all subsequent simulations.

Fig. 4. Mesh of the computational domain

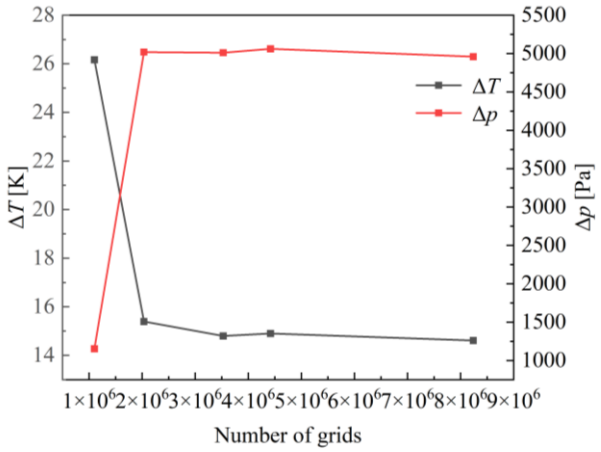

Fig. 5. Mesh independence verification for Hybrid fin

3.2. Model accuracy verification

Model reliability is validated against the experimental data of Liu et al. [25] under conditions summarized in Tab. 2. A simplified physical model with periodic boundaries replicates the channel arrangement within the PCHE. The hot-side sCO_2 temperature difference between inlet and outlet serves as the main validation parameter. Fig. 6, shows good agreement between the present numerical results and reported experimental data, confirming that the developed model can reliably predict PCHE flow and heat transfer behavior for subsequent analysis. The close agreement between the simulation results and experimental data for both temperature difference and pressure drop confirms that the present model accurately reproduces the conjugate heat transfer and fluid flow behavior within the hybrid-fin PCHE channels under sCO_2 conditions.

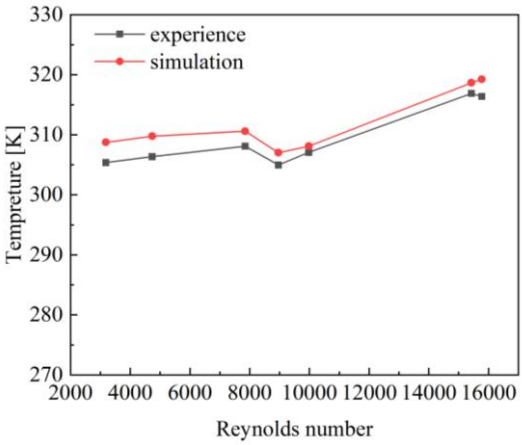

Fig. 6. Comparison of experimental and simulation results

Tab. 2. Boundary conditions for numerical model validation

Case	$m_{c,\,in}$ [kgs^{-1}]	$m_{h,\,in}$ [kgs^{-1}]	$p_{c,\,out}$ [MPa]	$p_{h,\,out}$ [MPa]	$T_{c,\,in}$ [K]	$T_{h,\,in}$ [K]
Case 1	0.0253	0.0897	0	8.41	293.15	320.57
Case 2	0.6053	0.3612	0	8.63	297.15	312.85
Case 3	0.5763	0.3073	0	8.7	297.15	318.70
Case 4	0.0236	0.0321	0	8.85	298.15	313.72
Case 5	0.2352	0.2381	0	8.92	298.02	312.02

4. Results and discussion

Based on the validated numerical model, the following section systematically analyzes the thermo-hydraulic performance of the three channel configurations. To balance heat transfer enhancement against pressure loss, the integrated performance metrics Nu/f and $Q/\Delta p$ are adopted, which simultaneously reflect thermal efficiency and hydraulic dissipation in compact heat exchanger design. In this study, Re, Nu and f are employed to evaluate the thermal-hydraulic performance, providing a theoretical basis for optimal design.

Fig. 7 compares streamline and velocity distributions across four cross-sections in three finned channels. The smooth airfoil fin induces local acceleration near its leading edge, enhancing near-wall mixing and thinning the thermal boundary layer through moderate flow separation. In contrast, the diamond fin maintains attached flow at the front but generates strong downstream recirculation due to its sharp edges, resulting in a thicker boundary layer and reduced heat transfer stability. The hybrid channel shows a more uniform velocity profile, centralizing high-speed flow in the core and suppressing

4.1. Local flow characteristics in the three channel configurations

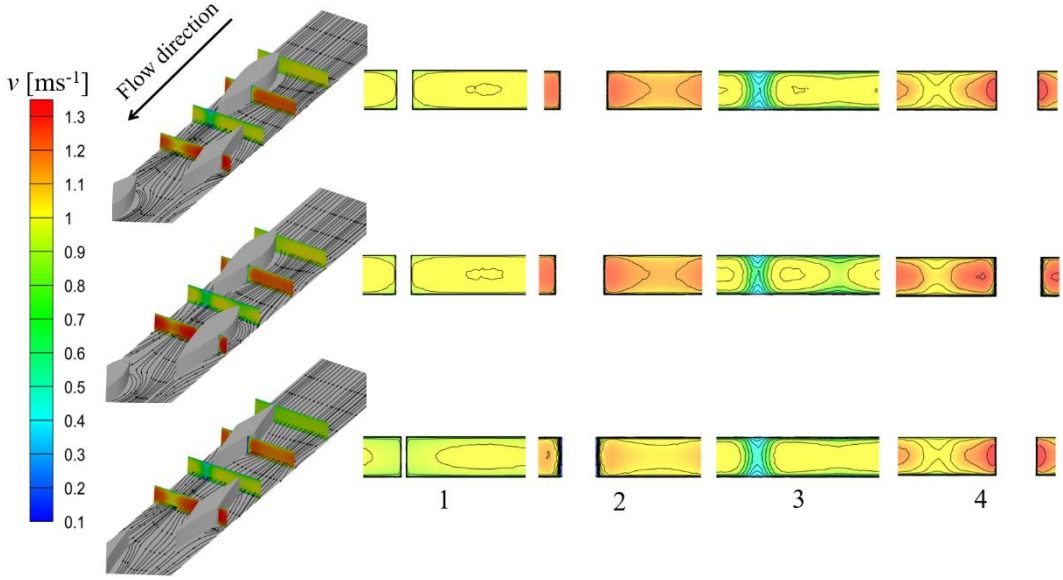

Fig. 7. Streamline and velocity cloud maps within the three channels

vortices. Unlike the airfoil fin's trailing-edge stagnation, the hybrid design reduces vortex intensity, thins the boundary layer, and distributes flow more evenly. These modifications—vortex suppression, boundary layer thinning, and flow uniformity—enhance convective heat transfer, increasing *Nu*. Concurrently, reduced recirculation and pressure loss improve the heat transfer–flow resistance balance, as seen in higher Nu/f and $Q/\Delta p$.

4.2. Temperature field and thermophysical property variations in the three channels configuration

Fig. 8 illustrates the temperature distribution across the three channel configurations, showing progressive cooling along the flow direction with the steepest gradient near the inlet. The hybrid-fin channel achieves the lowest outlet temperature and largest temperature drop about 15 K, whereas the airfoil-fin channel exhibits gradual cooling due to flow separation, and the diamond-fin channel displays localized enhancement but overall nonuniform distribution. Fig. 9 (a) quantitatively confirms these trends, with rapid temperature decline near the inlet followed by stabilization toward the outlet. Corresponding density variations in Fig. 9 (b) reveals an inverse relationship with temperature, with the hybrid channel achieving 1.7% and 1.2% higher density than the smooth airfoil and diamond configurations, respectively. This synergistic thermal and thermodynamic behavior occurs due to stronger flow disturbance and a thinner thermal boundary layer in the hybrid design, which enhance thermophysical gradients. Mechanisms such as vortex suppression and improved fluid mixing boost heat transfer while reducing pressure loss through flow uniformity. These fundamental characteristics result in higher overall Nu/f and $Q/\Delta p$ performance, providing the physical basis for the improved performance parameters observed in the hybrid configuration, as will be presented in the following section.

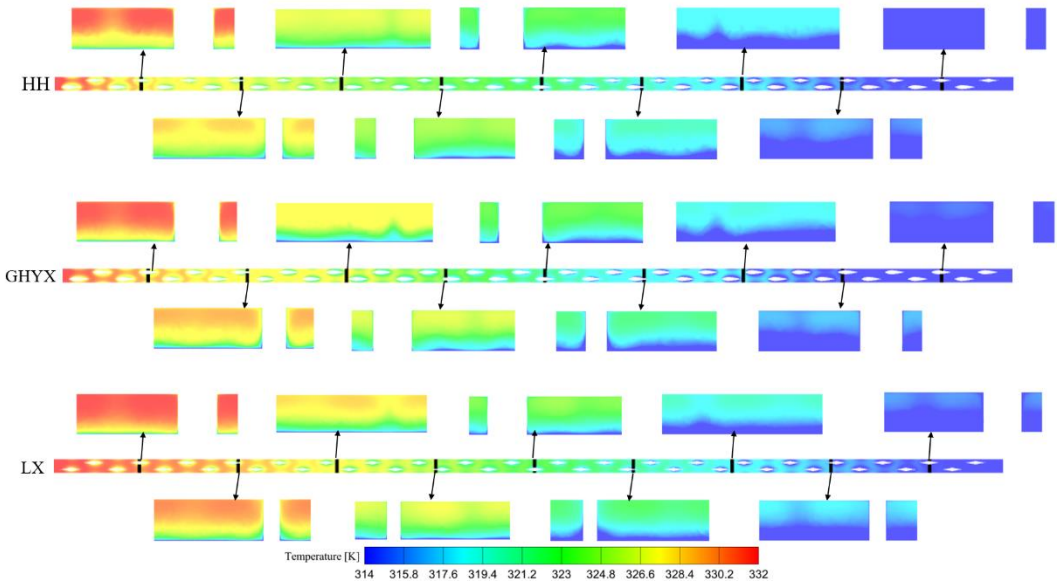

Fig. 8. Temperature distribution cloud maps of three different rib channels

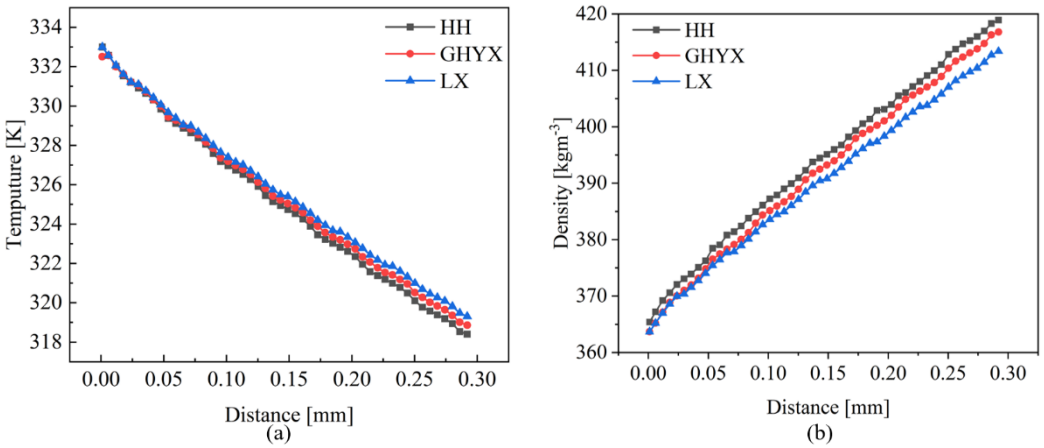

Fig. 9. Temperature and density changes along the hot fluid channel

4.3. Comprehensive comparison of heat transfer and flow resistance performance among the three channel configurations

Fig. 10 (a) presents the variation of the *Nu* with respect to the inlet mass flow rate for the three different fin configurations. As the inlet mass flow rate increases, *Nu* rises significantly in all cases. When the mass flow rate increases from 0.00121 kg/s to 0.00323 kg/s, the *Nu* values of the hybrid-fin channel are 9.2%, 7.4%, 6.1%, 5.7%, and 4.6% higher than those of the smooth airfoil-fin channel, and 16.5%, 14.3%, 12.7%, 11.2%, and 10.4% higher than those of the diamond-fin channel, respectively. This result indicates that the hybrid-fin structure effectively enhances the overall heat transfer performance of the PCHE. Fig. 10 (b) compares the variation of *f* with the inlet mass flow rate for the three channels. The *f* decreases with increasing flow rate for all structures. However, given the similar *f* values across the three configurations and the significantly higher heat transfer performance of the hybrid-fin channel, the hybrid-fin configuration achieves a synergistic optimization between heat transfer enhancement and flow resistance control, maintaining a rational balance between thermodynamic and hydrodynamic performance.

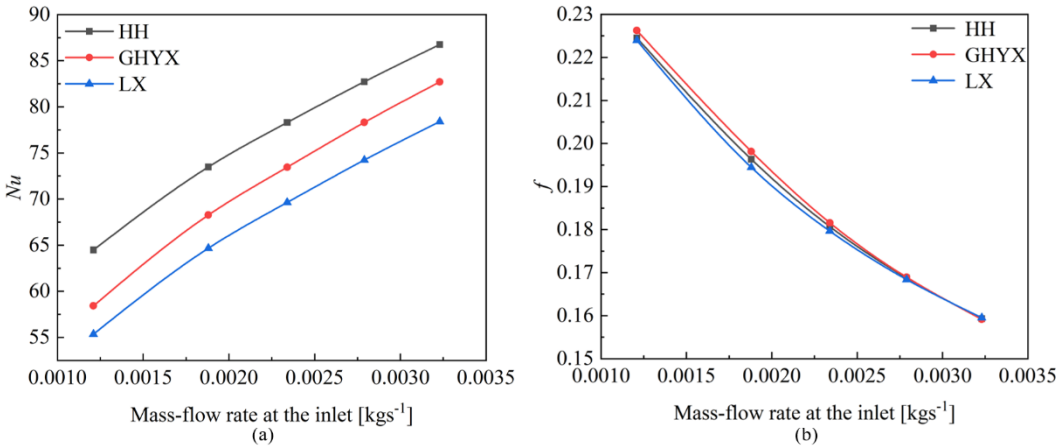

Fig. 10. Variation of *Nu* and *f* in different microchannel heat exchangers

Fig. 11 shows the variations of Δp with mass flow rate and *Nu* versus Δp for the three fin configurations. As illustrated in Fig. 11 (a), the *Nu* values of all channels increase with rising pressure drop, indicating that higher pressure difference enhances flow disturbance and, consequently, heat transfer. It is evident that the hybrid-fin channel outperforms both the diamond-fin and smooth airfoil-fin channels in terms of heat transfer performance under comparable pressure losses. When Δp is 4000 Pa, the *Nu* value of the hybrid-fin channel is 6.8% and 14.7% higher than those of the smooth airfoil-fin and diamond-fin channels, respectively. The staggered arrangement of different fin types in the hybrid configuration strengthens fluid turbulence and enhances mixing. As shown in Fig. 11 (b), the pressure drop of the hybrid-fin channel is only slightly higher than those of the other two structures. The optimized flow path in the hybrid-fin channel enhances flow disturbance while constraining resistance growth, ensuring superior thermo-hydraulic performance.

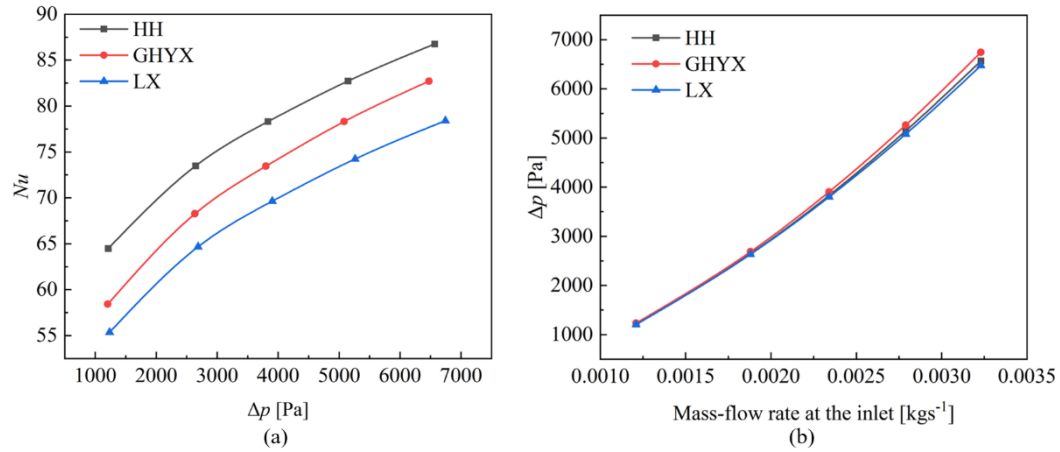

Fig. 11. Variation of *Nu* with Δp at different microchannel heat exchangers

The performance evaluation criteria, *Nu*/*f* and $Q/\Delta p$, are used to assess and compare the comprehensive performance of the three channels. Fig. 12 shows the variation of these two performance indices with inlet mass flow rate. As shown in Fig. 12 (a), the *Nu*/*f* values for all configurations increase with rising inlet mass flow rate, and the overall order is: Hybrid fin > Smooth airfoil fin > Diamond fin. Compared with the smooth airfoil-fin channel, the hybrid-fin configuration shows increase of 10.7%, 8.2%, 7.4%, 6.3%, and 5.7% in *Nu*/*f* at the five mass flow rates. Relative to the diamond-fin channel, the increases are 16.4%, 13.7%, 12.4%, 11.5%, and 9.8%, respectively. As shown in Fig. 12 (b), The

comprehensive thermo-hydraulic performance $Q/\Delta p$ decreases with increasing mass flow rate for all channels, reflecting that the growth rate of pressure loss outpaces heat transfer enhancement at higher velocities. Nevertheless, the hybrid-fin channel consistently achieves the highest $Q/\Delta p$ values. Specifically, it enhances $Q/\Delta p$ by 9.7%, 7.2%, 5.1%, 4.6%, and 2.3% relative to the smooth airfoil-fin channel, and by 33.5%, 16.2%, 12.7%, 8.4%, and 6.3% relative to the diamond-fin channel. This comparative analysis sustained superiority confirms that the hybrid design optimally balances thermal performance and flow resistance, delivering maximal heat transfer output per unit pressure loss. At higher velocities, pressure loss outpaces heat transfer enhancement due to thermal saturation, moderating performance gains. The hybrid-fin channel maintains superior performance among all configurations.

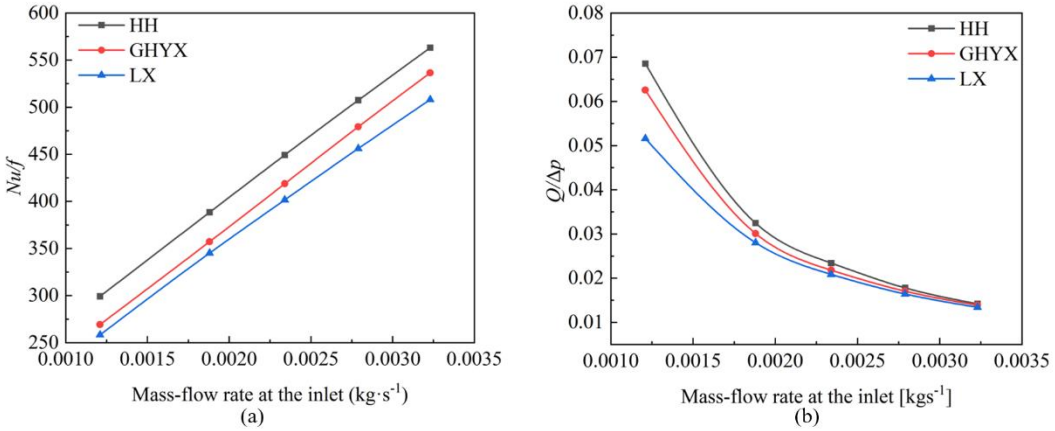

Fig. 12. Variation of *Nu*/*f* and *Q*/Δ*p* in different microchannel heat exchangers

5. Conclusions

This study proposes a novel hybrid-fin channel combining smooth airfoil and diamond fins to enhance the thermo-hydraulic performance of a sCO_2 printed circuit heat exchanger. Numerical simulations comparing the hybrid configuration with conventional single-fin designs under sCO_2 conditions yield the following conclusions:

(1) With in the *Re* range of 3200 to 7200, the hybrid channel achieves 16.5–10.4% and 9.2–4.6% higher *Nu* than the smooth airfoil and diamond fin channels, respectively.

(2) The alternating fin arrangement enhances thermal performance while maintaining flow efficiency, improving *Nu*/*f* by 5.7–10.7% and 9.8–16.4% over the two baseline designs, with corresponding $Q/\Delta p$ enhancements of 2.3–9.7% and 6.3–33.5%.

(3) The superior performance of the hybrid configuration is attributed to its ability to suppress vortex formation, thin the thermal boundary layer, and promote more uniform velocity distribution, thereby achieving a better synergy between heat transfer enhancement and pressure drop control.

A fundamental basis for optimizing fin arrangements in PCHE is established through a hybrid configuration, demonstrating strong potential for advancing compact heat exchangers in sCO_2 systems. The proposed hybrid-fin design is particularly suitable for applications requiring enhanced heat transfer with controlled pressure drop, such as sCO_2 Brayton cycles and industrial thermal management systems. To further the outcomes of this study, subsequent work can primarily focus on computational refinements, including systematic parametric analysis over an expanded geometric domain, and multi-objective optimization under variable operational regime.

Nomenclature

D_h	hydraulic diameter, [m]	T	temperature, [K]
f	friction factor, [$=\Delta p D_h/2\rho u^2 L$], [–]	*Greek Symbols*	
L_a	total width of the channel, [mm]	λ	thermal conductivity, [$Wm^{-1}K^{-1}$]
L_h	lateral spacing, [mm]	ρ	density, [kgm^{-3}]
L_s	longitudinal spacing, [mm]	*Subscripts*	
L_v	lateral spacing, [mm]	h, in	hot inlet
m	mass flow rate, [kgs^{-1}]	c, out	cold outlet
Nu	Nusselt number, [$=hD_h/\lambda$], [–]	Acronyms	
p	pressure, [Pa]	HH	hybrid channel
Δp	pressure drop, [Pa]	LX	diamond fin channels
Q	heat transfer rate, [W]	GHYX	smooth airfoil fin channels
Re	Reynold number, [$=\rho u D_h/\mu$], [–]	PCHE	printed circuit heat exchanger

Acknowledgements

This work was supported by Natural Science Foundation of Henan (Grant No. 252300423137).

References

[1] Huang, J., *et al*., Flow and heat transfer of He-Xe mixture in different ultra-compact heat exchangers, *Applied Thermal Engineering, 270* (2025), 126194.

[2] Iverson, B. D., *et al*., Supercritical CO_2 Brayton cycles for solar-thermal energy, *Applied Energy, 111* (2013), pp. 957-970.

[3] Garg, P., *et al*., Supercritical carbon dioxide Brayton cycle for concentrated solar power, *The Journal of Supercritical Fluids, 76* (2013), pp. 54-60.

[4] Gu, X., *et al*., Analysis of flow and heat transfer performance of different types of flow channels in printed circuit heat exchangers for pre-coolers, *Thermal Science, 28* (2024), 4, pp. 2977-2988.

[5] Haris, M., *et al*., Mixed convection analysis in a dual-driven cavity with a stable vertical temperature gradient using the Lattice Boltzmann method, *Thermal Science,* 29 (2025), 3B, pp. 2277-2296.

[6] Tian, Z., *et al*., Experimental study and dynamic response analysis of thermal–hydraulic characteristics in zigzag PCHE at ultra-low temperature, *Applied Thermal Engineering, 268* (2025), 125897.

[7] Zhang, Y., *et al*., Study on thermal-hydraulic performance of airfoil fin PCHE using vortex generators with different arrangement parameters for SCO_2 Brayton cycle, *Progress in Nuclear Energy, 185* (2025), 105724.

[8] Chu, W. X., *et al*., Experimental investigation on SCO_2-water heat transfer characteristics in a printed circuit heat exchanger with straight channels, *International Journal of Heat and Mass Transfer, 113* (2017), pp. 184-194.

[9] Figley, J., *et al*., Numerical study on thermal hydraulic performance of a printed circuit heat

exchanger, *Progress in Nuclear Energy, 68* (2013), pp. 89-96.

[10] Meshram, A., *et al*., Modeling and analysis of a printed circuit heat exchanger for supercritical CO_2 power cycle applications, *Applied Thermal Engineering, 109* (2016), pp. 861-870.

[11] Lee, S. M., Kim, K. Y., Comparative study on performance of a zigzag printed circuit heat exchanger with various channel shapes and configurations, *Heat and Mass Transfer, 49* (2013), 7, pp. 1021-1028.

[12] Ngo, T. L., *et al*., New printed circuit heat exchanger with S-shaped fins for hot water supplier, *Experimental Thermal and Fluid Science, 30* (2006), 8, pp. 811-819.

[13] Zhang, L., *et al*., A new structure of PCHE with embedded PCM for attenuating temperature fluctuations and its performance analysis, *Energy, 254* (2022), 124462.

[14] Hu, H., *et al*., Dynamic characteristics of the recuperator thermal performance in a S–CO_2 Brayton cycle, *Energy, 214* (2021), 119017.

[15] Zhang, H., *et al*., Experimental and numerical investigations of thermal-hydraulic characteristics in a novel airfoil fin heat exchanger, *International Journal of Heat and Mass Transfer, 175* (2021), 121333.

[16] Yang, Y., *et al*., Experimental study of the flow and heat transfer performance of a PCHE with rhombic fin channels, *Energy Conversion and Management, 254* (2022), 115137.

[17] Kim, T. H., *et al*., Numerical analysis of air-foil shaped fin performance in printed circuit heat exchanger in a supercritical carbon dioxide power cycle, *Nuclear Engineering and Design, 288* (2015), pp. 110-118.

[18] Chang, H., *et al*., Experimental study on heat transfer performance of sCO_2 near pseudo-critical point in airfoil-fin PCHE from viewpoint of average thermal-resistance ratio, *International Journal of Heat and Mass Transfer, 196* (2022), 123257.

[19] Cui, X., *et al*., Numerical study on novel airfoil fins for printed circuit heat exchanger using supercritical CO_2, *International Journal of Heat and Mass Transfer, 121* (2018), pp. 354-366.

[20] Wu, Y. Y., *et al*., Optimize the design analysis of hybrid fin structure microchannel heat exchanger, *Progress in Nuclear Energy, 175* (2024), 105333.

[21] Zhao, Z., *et al*., Numerical Investigation on the flow and heat transfer characteristics of supercritical liquefied natural gas in an airfoil fin printed circuit heat exchanger, *Energies, 10* (2017), 11, 1828.

[22] Xu, X. Y., *et al*., Thermal-hydraulic performance of different discontinuous fins used in a printed circuit heat exchanger for supercritical CO_2, *Numerical Heat Transfer, Part A: Applications, 68* (2015), 10, pp. 1067-1086.

[23] Gu, X., *et al*., Hybrid optimization for structure of printed circuit heat exchanger with airfoil fins, *International Journal of Thermal Sciences, 212* (2025), 109803.

[24] Ishaq, M., *et al*., Diamond-shaped extended fins for heat transfer enhancement in a double-pipe heat exchanger: an innovative design, *Applied Sciences-Basel, 11* (2021), 13, 5954.

[25] Liu, B., *et al*., Thermal-hydraulic performance analysis of printed circuit heat exchanger precooler in the Brayton cycle for supercritical CO_2 waste heat recovery, *Applied Energy, 305* (2022), 117923.

Received: 30.11.2025.
Revised: 11.02.2026.
Accepted: 23.02.2026.